

# Natural Gas Transfer Pump Fault Diagnosis on Multi-Sensor Fusion and Machine Learning

Xu-Bin Dong\*, Chen-Yong Li

School of Electronic Information  
Chongqing University of Engineering  
Chongqing 4001320, China  
xubindong0826@sina.com, 15111820484@163.com

Sofia Patel

College of information technology  
Waikato Institute of Technology  
Hamilton 3240, New Zealand  
qv6290@163.com

\*Corresponding author: Xu-Bin Dong

Received August 30, 2023, revised October 21, 2023, accepted December 28, 2023.

---

**ABSTRACT.** *Machine learning (ML) techniques have great engineering value in the field of natural gas transfer pump fault diagnosis. However, the traditional spectral analysis method is difficult to extract the characteristic components of the fault in transmission pump fault diagnosis. In addition, the existing fault diagnosis methods cannot accurately distinguish what fault mode the fault component belongs to. In order to solve the above problems, this paper proposes a natural gas transfer pump fault diagnosis method based on multi-sensor fusion and machine learning. Firstly, the vibration signals of the natural gas transfer pump are collected by multiple acceleration sensors, and the original data are processed by Complementary Ensemble Empirical Mode Decomposition (CEEMD) to obtain multiple vibration fault characteristic IMF components. Then, the IMF components are denoised by Tunable Q-factor Wavelet Transform (TQWT). As an improved method of wavelet transform, TQWT can obtain data that can express all the features of the original data with less noise by adjusting the Q-factor. Finally, the local and global kernel functions are linearly summed using weights to form a multi-core support vector machine to identify vibration fault features. The experimental results show that the combination of CEEMD and TQWT can effectively eliminate modal aliasing and obtain IMF components that clearly characterise fault features. Meanwhile, the fault diagnosis accuracy of the multicore support vector machine is improved from 77.5% to 87.6% compared with the existing methods.*

**Keywords:** Conveyor pump; Fault diagnosis; Empirical modal decomposition; Support vector machine; Acceleration sensor

---

**1. Introduction.** With the rapid development of the global natural gas industry, natural gas transfer pumps have been widely used and have now become an indispensable and important mechanical equipment in the process of natural gas extraction, transmission and pressurisation. However, transfer pumps may directly lead to failures during operation due to human factors or other factors. The occurrence of transfer pump failures can directly hinder the daily operation of the entire natural gas system [1, 2]. In order to reduce the economic property losses caused by natural gas transfer pump failures, it is urgent to research and develop advanced fault diagnosis techniques.

Currently, the core theory in the field of mechanical fault diagnosis is to judge or predict the state of mechanical operation by monitoring the state information in the process of mechanical operation and combining data analysis and mechanical fault theory. The purpose of mechanical fault diagnosis is to ensure that the power equipment can run stably for a long time and at full load [3, 4]. As mechanical equipment tends to be intelligent and precise, resulting in the production and manufacturing cost of mechanical equipment is also higher and higher. If the equipment is damaged, the repair cost will also be quite high. Being able to repair the faults in time when they first occur can minimise the repair costs.

In the early stage of the development of detection technology, people diagnosed faulty equipment based on their subjective experience [5]. Through sound perception or visual observation, people can rely on their past experience to diagnose the faulty equipment's working condition. This method does not have an objective theoretical basis, so there is no fixed model or principle to follow. Due to a strong subjective consciousness, the empirical analysis method often results in many detection errors [6]. With the continuous maturity of detection technology, expert systems, artificial neural network technology and support vector machine technology on fault diagnosis have been gradually developed [7, 8].

Mechanical fault diagnosis technology is a kind of multidisciplinary integration of science and technology, which has been developed rapidly in the 1960s thanks to the emergence of fast and efficient Fourier transform. Nowadays, the emerging signal analysis technology (filtering technology, spectral analysis technology) and intelligent control technology (expert system, neural network) are tried to be applied in the field of fault diagnosis, which has led to the increasing improvement of mechanical fault diagnosis technology. Mechanical fault diagnosis technology mainly includes two aspects of condition monitoring technology [9, 10] and fault diagnosis technology [11, 12]. Condition monitoring technology is mainly the application of certain means (such as sensors, signal collectors, etc.) to track and monitor the operating status of mechanical equipment [13]. Diagnostic technology, on the other hand, is to analyse the collected relevant information and judge the possible mechanical failure of the equipment according to the mechanical failure theory.

The main purpose of condition monitoring technology is to collect information related to the operating state of the equipment and provide a source of information for fault diagnosis technology. Fault diagnosis is usually achieved by studying and processing various parameters, which must be able to reflect the working state of various types of equipment, including vibration, heat, noise, current, power, speed and so on. Among them, the vibration signal and the detection of fault information is the basis of mechanical fault diagnosis. Vibration signals can intuitively reflect the fault-related characteristics and characterise the various indicators of equipment operation. Therefore, checking and identifying whether the vibration signals of natural gas transfer pumps are normal or not has become an important method for its fault diagnosis.

**1.1. Related Work.** Currently, natural gas transfer pumps are divided into two main categories: centrifugal pumps and reciprocating piston pumps. The object of this work is centrifugal pump. Centrifugal pumps use the centrifugal force of the impeller to raise the gas pressure, including single-stage centrifugal pumps and multi-stage centrifugal pumps. Centrifugal pumps are suitable for small and medium flow rates of natural gas.

When a centrifugal pump failure occurs, it must be accompanied by vibration. At the same time, the damage produced by long-term operation, all of which can cause abnormal operation, will also exacerbate the changes in vibration. Studies have shown

that vibration contains a large amount of information. Therefore, the vibration analysis method is commonly used in the current centrifugal pump fault diagnosis application [14]. The core content of vibration analysis method includes how to effectively collect information, analysis and processing of vibration signals, extraction of feature vectors, state identification and analysis, fault diagnosis and decision-making.

Fault diagnosis techniques based on vibration analysis methods can be divided into two types: 1) non-adaptive analysis methods and 2) adaptive analysis methods. Among the non-adaptive analysis methods, people often choose time-frequency analysis methods, such as Fourier transform, short-time Fourier transform, Wigner-Ville distribution, and wavelet transform, etc. Satpathi et al. [15] proposed a fault diagnosis method for DC transfer pumps based on short-time Fourier transform. Cheng et al. [16] proposed a short-time Fourier transform-based fault detection method for polymorphic switches. The short-time Fourier transform can traditionally make up for the shortcomings of the Fourier transform in analysing non-stationary signals, but the short-time Fourier transform has the problem of unchangeable resolution. Compared with other methods, wavelet transform is abler to directly characterise the local features of the signal in time and frequency, and there is more resolution. Wavelet transform can be used to analyse both smooth and non-smooth signals. Dong et al. [17] proposed a hob fault diagnosis method based on spectral wavelet transform and random forest. Wang et al. [18] proposed a bearing fault diagnosis method based on sparse bootstrap empirical wavelet transform. However, none of these methods can select the corresponding environmental factors based on the characteristics of the signal data itself, thus generating a cumulative error and causing a reduction in the accuracy of the system.

The Hilbert-Huang transform shows better advantages in dealing with nonlinear non-smooth signals. The Hilbert-Huang transform can be divided into two parts, one of which is Empirical Mode Decomposition (EMD), which achieves adaptive separation of signals. Sun et al. [19] proposed a bearing fault diagnosis method based on Empirical Mode Decomposition and Improved Chebyshev Distance. Hu and Li [20] proposed a rolling bearing fault diagnosis method based on adjustable envelope EMD and support vector machine. However, when the signal is not pure white noise, the EMD may suffer from modal aliasing due to the loss of some scales. This modal aliasing phenomenon changes the time-frequency distribution of the signal, making the physical meaning of the IMF components unclear, resulting in a significant reduction in the accuracy of the decomposition. In addition, the IMF component has a lot of noise on the low-frequency data, resulting in the traditional support vector machine cannot accurately distinguish what fault mode the fault component belongs to.

**1.2. Motivation and contribution.** Through the above analysis, it can be shown that compared with the non-adaptive method, the EMD-based adaptive method achieves a more excellent fault diagnosis effect on nonlinear signals. Therefore, in order to solve the modal aliasing problem of EMD and the low-frequency noise interference problem, a natural gas transfer pump fault diagnosis method based on multi-sensor fusion and machine learning is proposed.

The raw data are processed by Complementary Ensemble Empirical Mode Decomposition (CEEMD) to obtain multiple vibration fault characteristic IMF components. The IMF components are denoised by Tunable Q-factor Wavelet Transform (TQWT). The local and global kernel functions are linearly summed using weights to form a multi-core support vector machine to identify the vibration fault features.

The main innovations and contributions of this paper include:

(1) In order to solve the problem of modal aliasing that exists in the traditional EMD method in the signal processing process, the method of using CEEMD instead of EMD is proposed in order to solve the shortcomings in the EMD method, and its effectiveness is verified;

(2) By adjusting the Q-factor and r-factor, the application of TQWT technique in noise reduction of IMF components of vibration fault features is realised to reduce the interference of low-frequency noise;

(3) The local and global kernel functions are linearly summed using weights to form a multi-core support vector machine to identify vibration fault features, which helps to improve the accuracy of fault identification.

## 2. Causes and analyses of conveyor pump failures.

**2.1. Common failure types of transfer pumps.** The parts of conveyor pumps that are prone to failure under most working conditions are usually divided into three categories: bearings, rotors and stator coils. Among them, the chance of bearing failure is usually higher. Therefore, this paper focuses on the detection and diagnosis of bearing failures. The following are the research analyses of the causes of such failure characteristics. These analyses will be used as the theoretical basis for the subsequent fault detection research work.

Conveyor pumps typically have a range of different levels of vibration and noise during operation. These characteristics will change greatly when the transfer pump is in different working conditions. We can analyse these vibration frequency, noise size and other operating parameters, so as to determine whether the pump is working properly, or there may be parts of the failure. There are many faulty parts of induction transfer pumps, which can be roughly summarised into the following three categories [21, 22]:

(1) Stator faults: Common stator fault problems generally occur in the stator winding section. Stator winding faults belong to a kind of electrical faults. Stator faults can be divided into two categories, one is symmetrical and the other is asymmetrical;

(2) Rotor failures: common rotor failure problems occur mostly in the rotor winding section. The causes of rotor failures include manufacturing hazards, operational fatigue, thermal loads and electromagnetic shocks during start-up [23];

(3) Bearing failure: Mechanical damage on the surface of the bearing combination is the most common, in which rolling elements, cages, etc. are susceptible to corrosion and wear. The main function of bearings is to support the rotor of the transfer pump and reduce the friction coefficient during its movement. Bearings can ensure the accuracy of rotor rotation and are one of the most common and easily damaged parts in transfer pumps. The working condition of bearings is inseparable from the operating efficiency of transfer pumps.

**2.2. Bearing failure mechanism analysis.** Centrifugal pumps typically use two types of bearings, plain and rolling bearings. Sliding bearings have no difference between the inner and outer rings and no rolling element. Rolling bearings change the type of friction between two contact surfaces from sliding to rolling. There is a primary cause for any type of bearing failure, including wear, fatigue spalling, plastic deformation, bearing corrosion, fracture, and gluing.

The rolling bearing consists of four parts, as shown in Figure 1. When the bearing fails suddenly, we can monitor the signal. The vibration frequency is the characteristic frequency of the bearing itself. When there is an abnormality in the bearing, there will be a series of shocks on a certain frequency, which is called the failure frequency of the

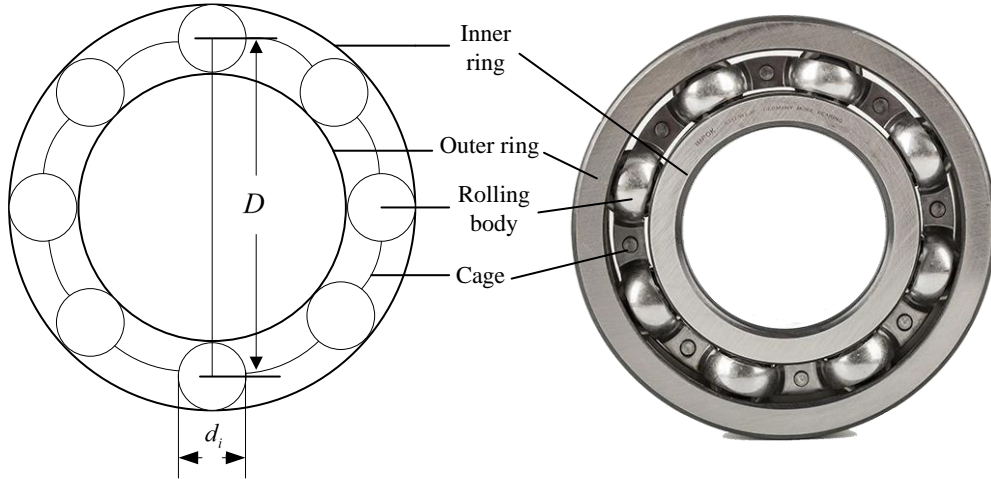


Figure 1. Rolling bearing structure of conveyor pumps

bearing. The monitoring of this failure frequency and its analysis of the data is the key issue in identifying bearing failures.

If the pitch diameter of the bearing is set to  $D$  (the pitch diameter refers to the diameter of the circle formed by the centre points of the rollers in the ideal operating condition), the diameter of the rolling element  $d$ , the outer diameter of the bearing  $r_1$ , the inner diameter of the bearing  $r_2$ , the contact angle  $\alpha$ , the number of rolling elements in the rolling bearing  $N$ , and the rotational frequency  $f_r$ , then the characteristic frequency of the rolling bearing can be expressed using the following methods.

The bearing characteristic frequency  $f_a$  in the event of an inner ring failure is shown below:

$$f_a = \frac{N}{2} \left[ 1 + \frac{d}{D} \cos \alpha \right] f_r \quad (1)$$

The bearing characteristic frequency  $f_b$  in the event of an outer ring failure is shown below:

$$f_b = \frac{N}{2} \left[ 1 - \frac{d}{D} \cos \alpha \right] f_r \quad (2)$$

The characteristic frequency  $f_c$  in the event of a rolling body failure is represented as shown below:

$$f_c = \frac{N}{2d} \left[ 1 - \left( \frac{d}{D} \right)^2 \cos^2 \alpha \right] f_r \quad (3)$$

The rotation frequency of the cage is  $f$ .

$$f = \frac{1}{2} \left[ 1 - \frac{d}{D} \cos \alpha \right] f_r \quad (4)$$

As you can see from the formula above, the failure characteristic frequency values are usually small, ranging from tens to hundreds of Hertz. When a bearing fails, the rotating shaft begins to run slightly, which causes the air gap of the centrifugal pump to become unbalanced. The magnetic flux flowing through the air gap will then also be affected. We can sense the corresponding harmonic current components within the coil windings of the stator section. The relationship between the harmonic current frequency and the vibration frequency is shown below.

$$f_d = |f_1 + kf_v| \quad (5)$$

where  $k$  is the frequency of the external power supply, and  $f_v$  is one of the characteristic frequencies of vibration when the bearing is abnormal.

By studying the digital indicators under these two signals, bearing faults can be detected precisely. The converted frequency domain information is compared with its intrinsic frequency to determine whether the bearing is faulty or not.

### 3. Fault feature extraction for transfer pumps based on CEEMD-TQWT.

**3.1. Data acquisition with traditional empirical model decomposition.** Three-dimensional acceleration sensors are chosen as the sensors for data acquisition in order to directly represent the vibration of the conveyor pump bearings in x-axis, y-axis and z-axis. Since the conveyor pump vibration signals are non-stationary signals, most of the methods use EMD to decompose the data as follows [24, 25]:

Step 1: Assuming that the observed signal is  $x(t)$ , find all the extreme points of the signal  $x(t)$ ;

Step 2: Fit the upper and lower envelope curves;

Step 3: Obtain the mean curves  $m_i(t)$  of the upper and lower envelopes;

$$m_i(t) = \frac{x_{\min}(t) + x_{\max}(t)}{2} \quad (6)$$

Determine whether  $h_i(t)$  satisfies the conditions of the IMF, if so, perform Step 4. If not, replace  $x(t)$  with  $h_i(t)$  and repeat the above steps until  $h_i(t)$  satisfies the criteria.

Step 4: Calculate the margin  $r_i(t)$ ;

$$r_i(t) = x(t) - c_i(t), \quad c_i(t) = h_{ik}(t) \quad (7)$$

Step 5: Determine whether  $r_i(t)$  is a single signal, if yes, the whole decomposition process is finished. Otherwise, replace  $x(t)$  with  $r_i(t)$  and repeat the above steps until  $r_i(t)$  meets the judgement condition;

After the EMD method the original signal  $x(t)$  is decomposed into a linear superposition:

$$x(t) = \sum_{i=1}^N c_i(t) + r_n(t) \quad (8)$$

where  $N$  denotes the total number of IMFs,  $c_i(t)$  denotes the  $i$ -th IMF component, and  $r_n(t)$  denotes the remaining component after multiple iterations.

It can be seen that EMD has good adaptive properties. Wavelet analysis requires a known basis function to be selected before application. However, unlike wavelet analysis, EMD only needs to decompose the features of the signal itself to obtain the IMF components of the frequencies. When the signals being decomposed are different, the frequencies of the IMF components obtained by the decomposition also differ. The EMD decomposition method is outstanding in nonlinear and nonsmooth processing.

**3.2. CEEMD.** Numerous research results have shown [26] that the white noise is decomposed by EMD, and the uniformly distributed frequency components contained in it are regularly separated. However, when the signal is not pure white noise, modal aliasing may occur in EMD due to the loss of some scales, which is due to the fact that the nature of EMD is a binary filter. The modal aliasing problem in EMD changes the time-frequency distribution of the signal, and the physical significance of each component of the IMF becomes less clear, resulting in a significant reduction in the accuracy of the decomposition.

In order to solve the problem of modal aliasing that exists in the classical EMD, researchers try to add more white noise and obtain some suppression effect. However, it

is not possible to add white noise indefinitely in practice, which will greatly increase the computational volume and lead to a long decomposition time. As an improved EMD method, CEEMD [27] can not only effectively suppress the modal aliasing, but also improve the computation speed to a certain extent. The specific implementation steps of the CEEMD method are as follows:

Step 1: Assume that the input signal is  $x(t)$ . The white noise amplitude to be added is initialised and decomposed  $m$  times using EMD. A pair of additive and subtractive noise signals (same amplitude and opposite phase) are added to the original signal  $x(t)$  to obtain:

$$\begin{cases} H_m(t) = x(t) + n_m(t) \\ J_m(t) = x(t) - n_m(t) \end{cases} \quad (9)$$

where  $n_m(t)$  denotes the  $m$ -th added white noise.

Step 2: Take the signals  $n_m(t)$  and  $J_m(t)$  as objects and apply EMD to decompose them so as to obtain the IMF components of both of them, as shown in the following procedure.

$$\begin{cases} H_m(t) = \sum_{j=1}^q c_{j,m}^+(t) \\ J_m(t) = \sum_{j=1}^q c_{j,m}^-(t) \end{cases} \quad (10)$$

where  $c_{j,m}^+$  and  $c_{j,m}^-$  both denote the  $j$ -th IMF obtained after decomposing the signal and  $q$  is the number of IMFs.

Step 3: Calculate the average of the IMF components obtained from  $M$  decompositions.

$$c_j = \frac{1}{2M} \sum_{m=1}^M (c_{j,m}^+(t) + c_{j,m}^-(t)) \quad (11)$$

Since EMD will have the problem of modal aliasing when processing the signal, which will lead to the loss of some information of the signal. Therefore, in this paper, CEEMD is chosen to process the vibration signals of conveyor pumps and evaluate and analyse the signals in two directions, namely, stability and time. Different frequencies correspond to different feature signals and represent the local information of the original signal, and there is aliasing between the IMF components, which means that the same IMF component is mixed with different frequency components. This phenomenon makes the time-frequency distribution of the signal unclear, and therefore cannot effectively restore the feature information of the original signal.

In order to verify the existence of modal aliasing in EMD, three components, IMF5, IMF6 and IMF7, were selected and processed by EMD and CEEMD, respectively. The IMF spectra obtained by the two methods are shown in Figure 2 and Figure 3, respectively.

From Figure 2, it can be seen that there is a cross overlap in the spectrum corresponding to IMF5, IMF6 and IMF7, which is not conducive to fault feature extraction for conveyor pumps. From Figure 3, it can be seen that CEEMD is able to reduce the frequency overlap and reduce the internal confusion of EMD. The number of crossings of IMF components in the spectrogram is significantly reduced, which verifies the superiority of CEEMD processing.

In order to further illustrate the efficiency of CEEMD, time calculations are performed for both treatments separately and the comparison results are shown in Figure 4. From Figure 4, it can be seen that the difference in time consumed by EMD and CEEMD is small and belongs to the same order of magnitude. Although, the calculation time of CEEMD is longer than that of EMD, the results are more accurate.

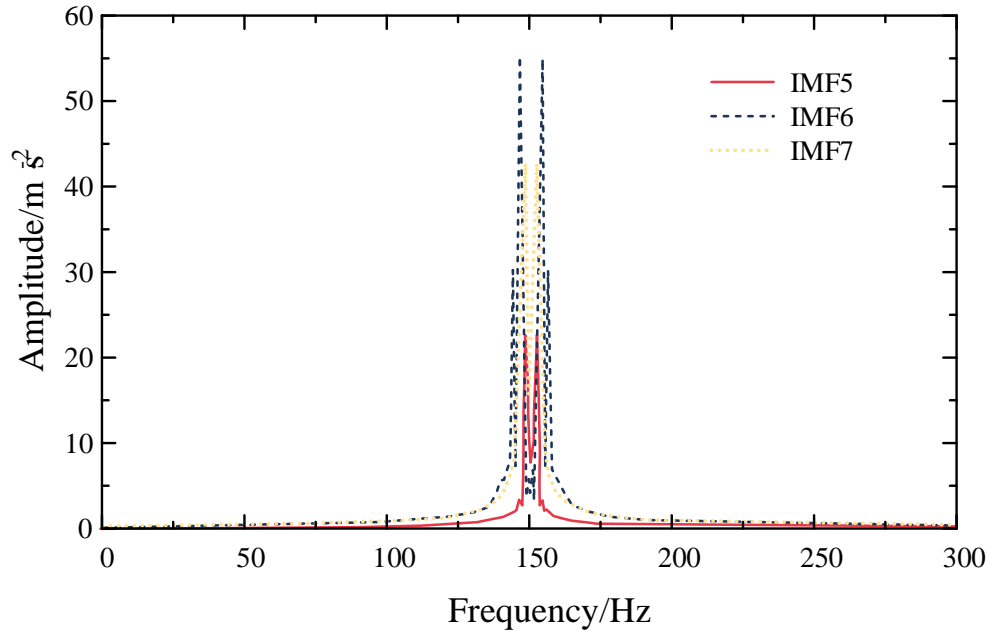


Figure 2. EMD processed IMF spectra

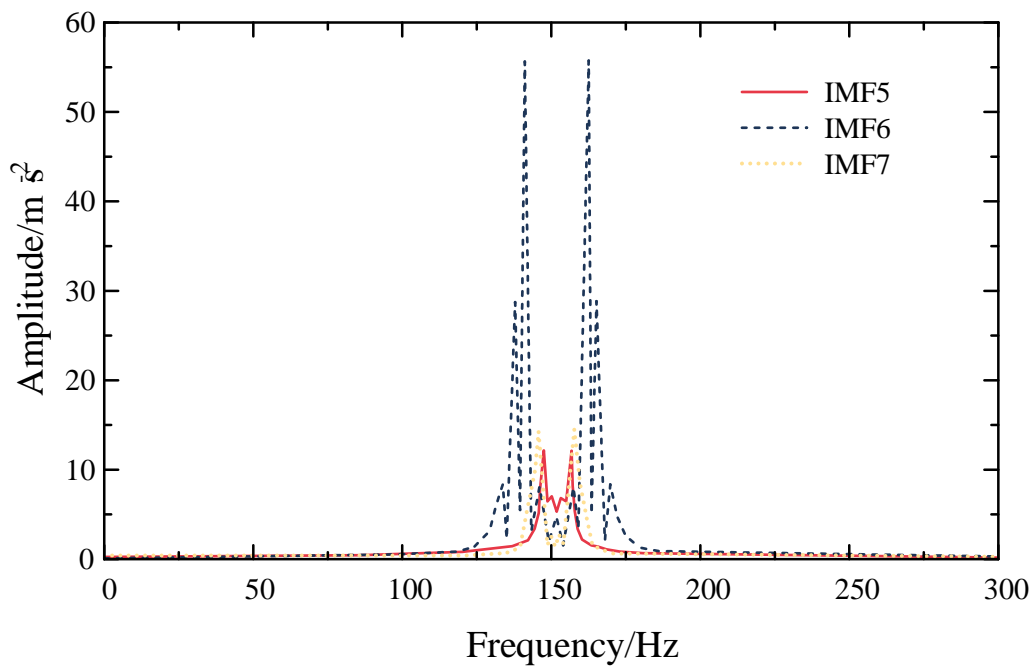


Figure 3. IMF spectrum after CEEMD processing

**3.3. TQWT.** As a novel time-frequency analysis method, the tunable quality factor wavelet transform (TQWT) [28, 29] realises the scale decomposition of non-smooth signals on wavelet bases with different quality factors by means of the iterative operation of two-channel filters and the fast Fourier transform. The TQWT overcomes the disadvantage of the constant quality factor of the traditional wavelet transform with full reconstructibility and completeness. As an improved method of wavelet transform, TQWT can obtain data that can express all the characteristics of the original data with less noise by adjusting the  $Q$  factor.

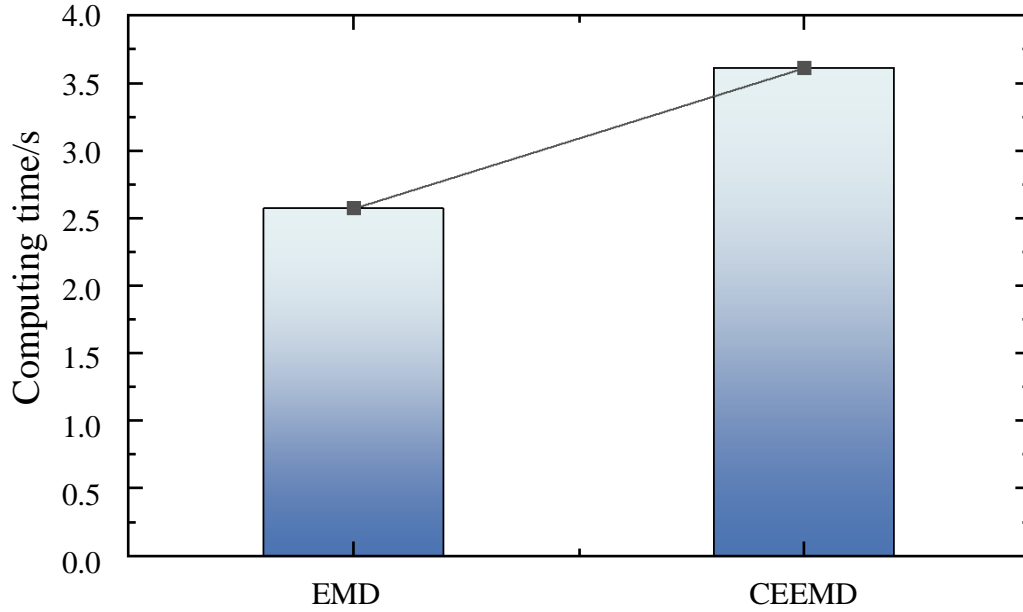


Figure 4. Calculation times for different methods

The  $Q$  factor (Quality Factor), is a physical quantity used to describe the damping of a system of oscillators in physics. The magnitude of the  $Q$  factor reflects the speed of oscillation of a signal's time-domain waveform. The  $Q$  factor is usually expressed as the ratio of the resonance frequency to the resonance frequency bandwidth, and is a dimensionless quantity.

$$Q = \frac{f_0}{\Delta f} \quad (12)$$

where  $f_0$  is the resonance frequency and  $\Delta f$  is the bandwidth of the resonance frequency.

Figure 5 depicts the time-domain waveform and frequency-domain distribution of the signal when the  $Q$  factor is 1 and 3, respectively. It can be seen that when the  $Q$  factor is 3, the time-domain waveform of the signal oscillates faster and the focusing in the frequency domain is better, while when the  $Q$  factor is 1, the time-domain waveform of the signal oscillates slower and the focusing in the frequency domain is worse. This shows that the magnitude of the  $Q$  factor reflects the speed of the oscillation of the signal waveform in the time domain and the focusing of the signal in the frequency domain.

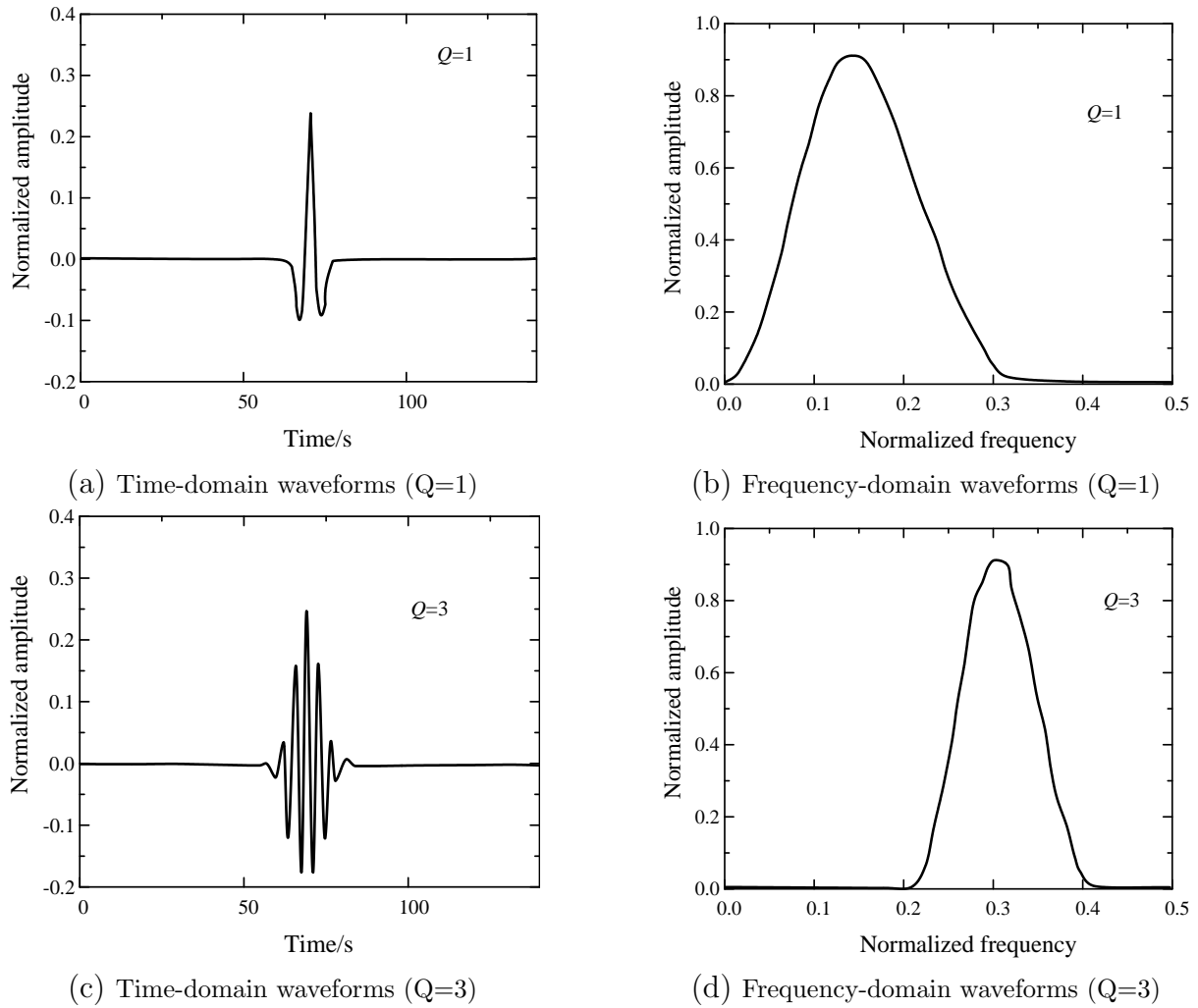


Figure 5. Time-domain waveforms and frequency-domain distributions

Taking the 3-layer decomposition reconstruction as an example, the TQWT can be represented as a two-channel decomposition filter bank, as shown in Figure 6. Compared

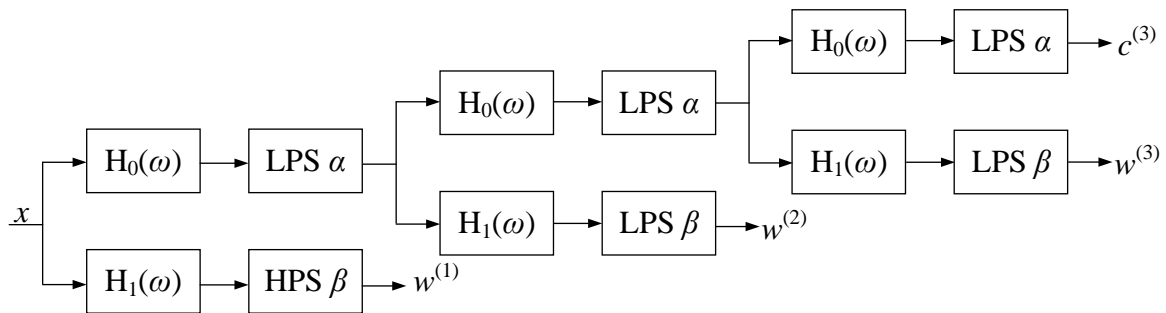


Figure 6. Decomposition filtering

with the traditional constant quality factor wavelet transform, the biggest advantage of TQWT is that its quality factor can be freely adjusted. Setting the quality factor of TQWT as  $Q$  and the redundancy factor as  $r$ , the number of decomposition layers  $j$  is the maximum value allowed by the theory, which is calculated as shown in the following

formula [30]:

$$j = \frac{\lg\left(\frac{N_s}{4(Q+1)}\right)}{g\left(\frac{Q+1}{Q+1-\frac{2}{r}}\right)} \quad (13)$$

where  $N_s$  is the signal length.

In order to retain the original data information, the noise must be smoothed. Therefore, this paper reduces the characteristic data noise of transfer pump through TQWT processing, which is able to smooth the noise amplitude at low frequency, effectively retaining the characteristics of the original data, and providing better data preparation for subsequent troubleshooting processing.

**4. Multi-core SVM based fault diagnosis of conveyor pump system.** Traditional SVM will choose a certain kernel function for different application scenario requirements. But such a model will lead to a weak generalisation ability of SVM learning, which cannot cope with the complex conveyor pump data sample situation.

Therefore, the fault diagnosis method based on traditional SVM cannot accurately distinguish what fault mode the fault component belongs to. Since the combined kernel has the ability to map data from multiple kernel functions, SVM based on combined kernel functions can better cope with real case requirements.

Multi Kernel SVM (MKSVM) solves the problem of blindness in the construction of kernel function and the selection of parameters of traditional SVM in fault diagnosis. Therefore, in this paper, MKSVM is used to classify the data, thus optimising the SVM and further improving the diagnostic accuracy. In this paper, the local and global kernel functions are linearly summed using weights to form a multikernel SVM, in which the combined kernel function  $K(x, z)$  is:

$$K(x, z) = \sum_{j=1}^M \beta_j k_j(x, z), \beta \geq 0, \sum_{j=1}^M \beta_j = 1, j = 1, 2, \dots, M \quad (14)$$

where  $\beta_j$  denotes the weighting factor and  $k_j(x, z)$  denotes the single kernel function.

Compared with the single kernel function learning method, the combined method can obtain higher classification accuracy and sample generalisation ability.

Substituting the kernel function into the decision function for classification gives:

$$f(x) = \text{sgn}\left(\sum_{i=1}^m \alpha_i y_i K(x_i, z_i) + b\right) \quad (15)$$

The definition of the decision function of the linear weighted MKSVM is shown below:

$$f(x) = \text{sgn}\left(\sum_{i=1}^m \sum_{j=1}^M \alpha_i y_i \beta_j K(x_i, z_j) + b\right) \beta_j \geq 0, \sum_{j=1}^M \beta_j = 1 \quad (16)$$

In this paper, the global kernel function POLY and the locality kernel function RBF are chosen to form the combined kernel function, thus taking into account both global and local sample features. Therefore, the combined kernel function  $K(x, z)$  can be expressed as:

$$K(x, z) = \beta_{RBF} k_{RBF}(x, z) + \beta_{POLY} k_{POLY}(x, z) \quad (17)$$

$$\beta_{RBF} + \beta_{POLY} = 1 \quad (18)$$

where  $\beta_{POLY}$  and  $\beta_{RBF}$  denote the weight factors of the global kernel function POLY and the localised kernel function RBF, respectively.

## 5. Experiments and analysis of results.

5.1. **Experimental environment.** The diesel transfer pump is used as the object of the fault diagnosis study to validate the transfer pump fault diagnosis method (CEEMD + TQWT + MKSVM) proposed in this paper.

The diesel transfer pump used in the experiment is shown in Figure 7, and its main parameters are shown in Table 1. Experimental process: (1) use multiple acceleration sensors to collect the vibration signals of the diesel transfer pump, with the parameters shown in Table 2; (2) perform CEEMD operation on the screened information in order to refine the vibration signals according to the time scale, making the typical signal information more prominent; (3) select the best combination of parameters from the point of view of signal noise reduction, and perform TQWT processing on the feature data obtained from the CEEMD processing; (4) use MKSVM analysis to analyse the feature vectors required for MKSVM. TQWT processing, in order to obtain the feature vectors required by MKSVM; (4) use MKSVM analysis to identify the state of the conveyor pump bearing signals. The TQWT algorithm has a quality factor  $Q = 1$  and a redundancy factor  $r = 1$ .

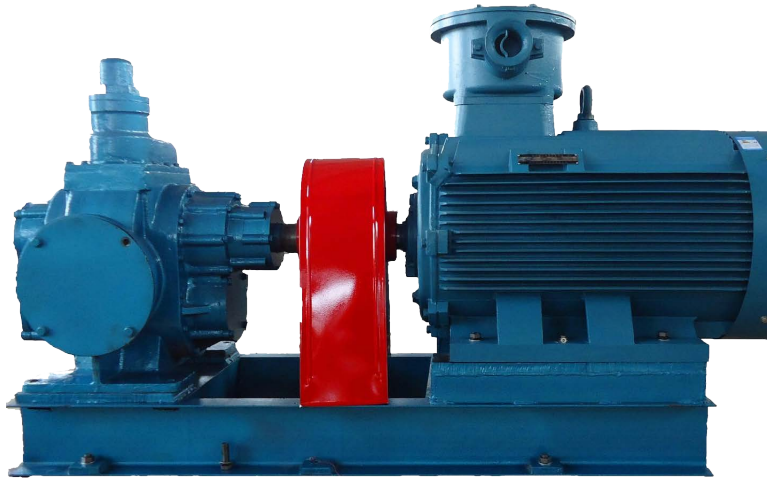


Figure 7. Natural gas transfer pumps used in the experiment

Table 1. Main Parameters of Diesel Engine

Parametric	Numerical value
Model number	WP6D180E201
Input voltage	380 V
Typology	centrifugal pumps
Discharge calibre	40 mm
Power (output)	4 kw
Flow rate	$10 \text{ m}^3/h$

The vibration signal of the diesel engine shown in Figure 8 shows that the regularity of the diesel engine shock characteristics is more obvious, and the frequency band distribution is stable, so there is no abnormal situation of the diesel engine.

From Figure 9 diesel engine vibration signal found that the regularity of the diesel engine impact characteristics is obvious, the high-frequency band shows the unique vibration characteristics of reciprocating machinery, industrial frequency and its harmonic

Table 2. Acceleration Sensor Parameters

Parametric	Numerical Value
Model number	ACC326 Triaxial Digital Accelerometer
Signal type	RS232/RS485/TTL
Supply voltage	9V-36V
Resolution (of a photo)	0.01g
Operating temperature	-40°C-85°C

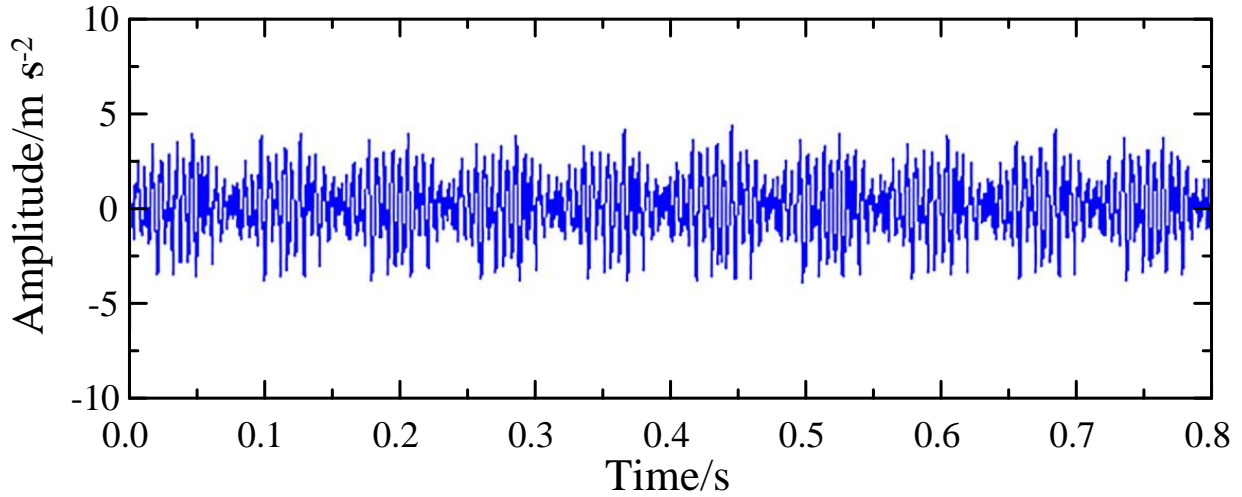


Figure 8. Diesel Engine Vibration Signal (no abnormality)

components appear in the low-frequency band, indicating that the bolts may be signs of loosening.

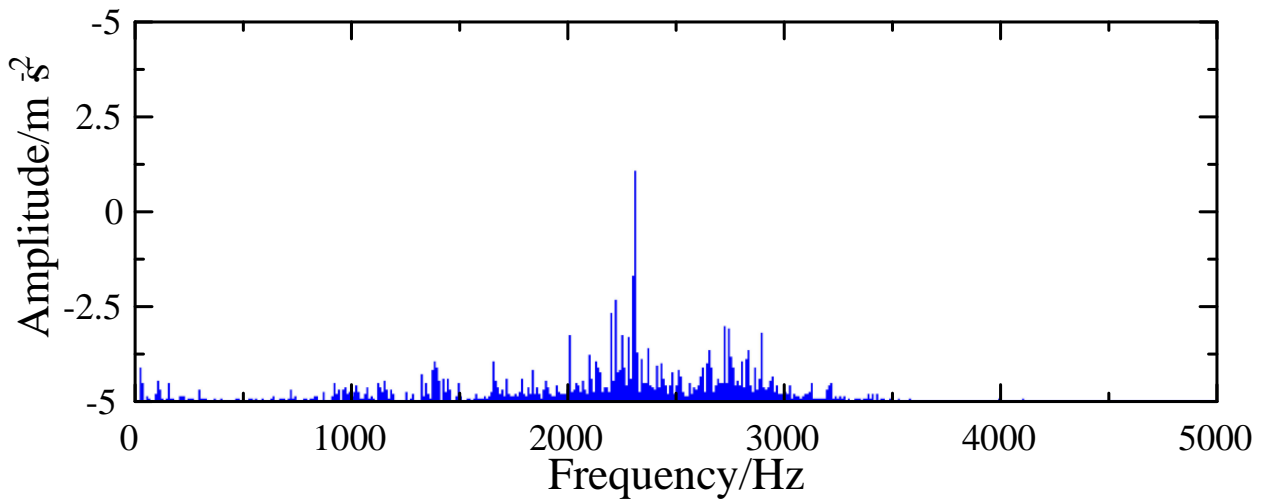


Figure 9. Diesel Engine Vibration Signal (Abnormal)

All signals were decomposed by CEEMD and 34 sets of decomposition results were obtained for the four working conditions, as shown in Table 3.

**5.2. Multiple kernel function combination tests.** In order to verify the optimal parameter settings for combining multiple kernel functions to classify the recognition

Table 3. CEEMD decomposition for four operating conditions

state of affairs	IMF1	IMF2	IMF3	IMF4	IMF5	IMF6	IMF7
1	0.73	0.534	0.639	0.516	0.258	0.096	0.069
2	1.617	1.152	0.659	0.489	0.366	0.171	0.074
3	0.83	0.799	0.634	0.584	0.297	0.174	0.036
4	1.198	0.851	0.633	0.577	0.345	0.18	0.054

model, 50 repetitions of the test were conducted for multiple combinations of kernel functions. The results of performance comparison of multiple kernel functions are shown in Table 4.

Table 4. Multicore Function Performance Comparison

kernel function (math.)	Kernel function parameter values	Accuracy/per cent
RBF core + POLY core	$\alpha = 4.5, d = 2$	85.3
RBF core + POLY core	$\alpha = 4.5, d = 3$	87.6
RBF core + RBF core	$\alpha = 4.5, d = 4.5$	76.5
POLY core + POLY core	$d = 4.5, d = 2$	72.2

As can be seen from Table 4, the accuracy of MKSVM is significantly improved compared to the single kernel function SVM. Moreover, when the value of the kernel function parameter is  $\alpha = 4.5$  and  $d = 3$  (RBF kernel+POLY kernel), MKSVM has the highest classification accuracy.

**5.3. Diagnostic performance comparison.** To further validate the performance of the proposed CEEMD + TQWT + MKSVM diagnostic method, it was compared with SVD + LMD + SVM [31], SVD + EMD + SVM [32], and EMD + TQWT + LSSVM [33], which were trained with 400 samples. The results of the comparison of the diagnostic performance of different methods are shown in Table 5 and Figure 10, where the kernel function parameters take the values of  $\alpha = 4.5$  and  $d = 3$ .

Table 5. Comparison of Accuracy of Different Methods

arithmetic	Accuracy of fault diagnosis/per cent	Time/s
SVD+LMD+SVM	77.5	4.7
SVD+EMD+SVM	78.4	4.8
EMD+TQWT+LSSVM	82.1	5.3
CEEMD+TQWT+MKSVM	87.6	5.7

From Table 5 and Figure 10, it can be seen that the EMD-based SVM diagnosis method has a better accuracy rate compared to the LMD-based SVM diagnosis, which is due to the fact that the EMD exhibits better robustness. Moreover, among the EMD-based SVM diagnosis methods, the CEEMD + TQWT + MKSVM method has the highest recognition rate, and the conveyor pump fault diagnosis accuracy reaches 87.6%. This is because CEEMD is an improved EMD method that can effectively suppress EMD modal aliasing without significantly increasing the computational complexity. Meanwhile, TQWT effectively removes the low-frequency noise. In addition, it can be seen that compared with other diagnostic methods, the method in this paper has some sacrifices in

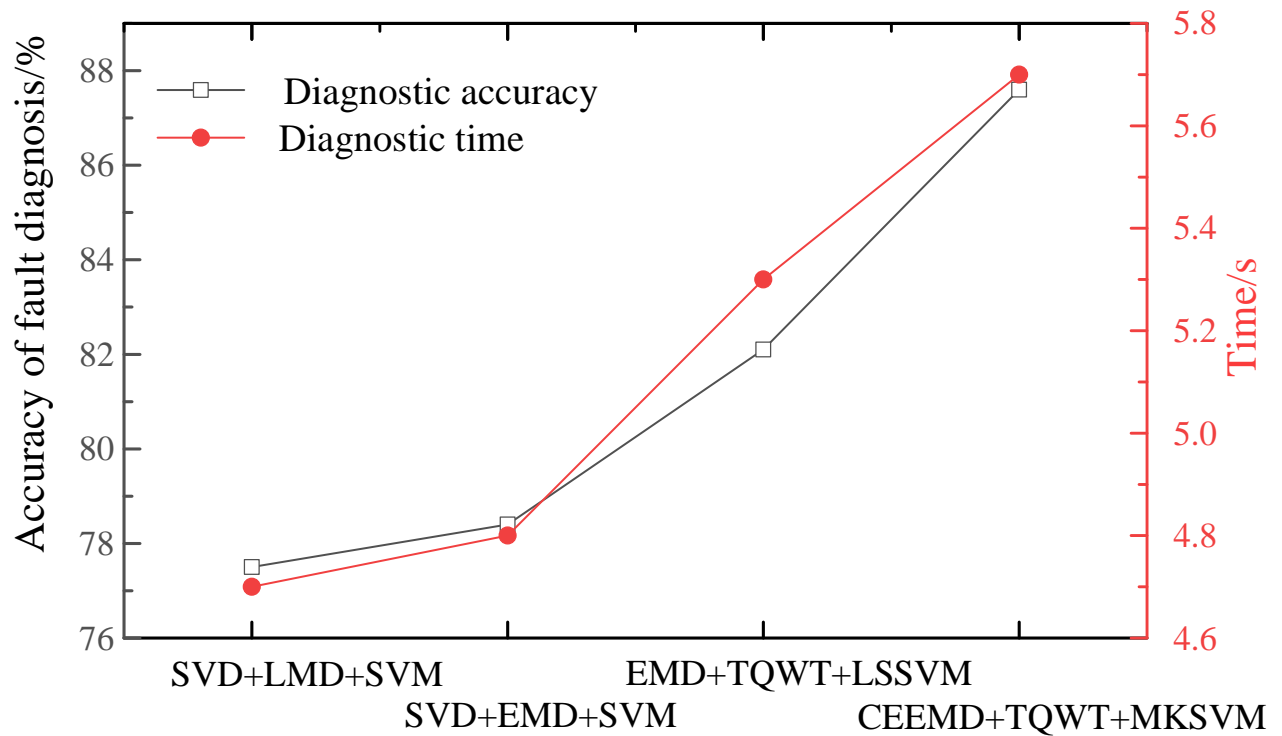


Figure 10. Comprehensive performance comparison of different methods

terms of time efficiency, because of the use of more complex combined kernel functions, and the judgement of the solution time is increased to a certain extent.

**6. Conclusion.** Aiming at the modal aliasing problem of EMD and the low-frequency noise interference problem, a natural gas transfer pump fault diagnosis method based on CEEMD + TQWT + MKSVM is proposed. Multiple vibration fault characteristic IMF components are obtained by processing the raw data using CEEMD. The IMF components are denoised by TQWT. The local and global kernel functions are linearly summed using weights to form a multikernel SVM to identify the vibration fault features. The results show that the combination of CEEMD and TQWT can effectively eliminate modal aliasing and obtain IMF components that clearly characterise fault features. Meanwhile, compared with the existing methods, the fault diagnosis accuracy of multicore SVM is improved from 76.7% to 83.1%. CEEMD suppresses mode aliasing to a certain extent, but there is a lack of theoretical selection basis for the setting of the optimal white noise parameters in the EMD decomposition method. Therefore, the follow-up study is to carry out an in-depth research on this issue.

**Funding Statement.** This work was supported by Chongqing Education Commission Science and Technology Research Program project (No. KJQN202301913) and Chongqing Natural Science Foundation project (No. cstc2021jcyj-msxmX0921).

## REFERENCES

- [1] Y. Ma, Y. Peng, and T.-Y. Wu, "Transfer learning model for false positive reduction in lymph node detection via sparse coding and deep learning," *Journal of Intelligent & Fuzzy Systems*, vol. 43, no. 2, pp. 2121-2133, 2022.

- [2] F. Zhang, T.-Y. Wu, J.-S. Pan, G. Ding, and Z. Li, "Human motion recognition based on SVM in VR art media interaction environment," *Human-centric Computing and Information Sciences*, vol. 9, no. 1, 40, 2019.
- [3] F. Zhang, T.-Y. Wu, Y. Wang, R. Xiong, G. Ding, P. Mei, and L. Liu, "Application of Quantum Genetic Optimization of LVQ Neural Network in Smart City Traffic Network Prediction," *IEEE Access*, vol. 8, pp. 104555-104564, 2020.
- [4] D. Xiao, C. Qin, H. Yu, Y. Huang, and C. Liu, "Unsupervised deep representation learning for motor fault diagnosis by mutual information maximization," *Journal of Intelligent Manufacturing*, vol. 32, no. 2, pp. 377-391, 2020.
- [5] Y. Liang, B. Li, and B. Jiao, "A deep learning method for motor fault diagnosis based on a capsule network with gate-structure dilated convolutions," *Neural Computing and Applications*, vol. 33, no. 5, pp. 1401-1418, 2020.
- [6] X. Zhao, J. Wu, Y. Zhang, Y. Shi, and L. Wang, "Fault diagnosis of motor in frequency domain signal by stacked de-noising auto-encoder," *Computers, Materials & Continua*, vol. 57, no. 2, pp. 223-242, 2018.
- [7] K. Wang, C.-M. Chen, Z. Liang, M. M. Hassan, G. M. L. Sarné, L. Fotia, and G. Fortino, "A trusted consensus fusion scheme for decentralized collaborated learning in massive IoT domain," *Information Fusion*, vol. 72, pp. 100-109, 2021.
- [8] F. Wang, R. Liu, Q. Hu, and X. Chen, "Cascade convolutional neural network with progressive optimization for motor fault diagnosis under nonstationary conditions," *IEEE Transactions on Industrial Informatics*, vol. 17, no. 4, pp. 2511-2521, 2021.
- [9] C.-Y. Lee, and M.-S. Wen, "Establish Induction Motor Fault Diagnosis System Based on Feature Selection Approaches with MRA," *Processes*, vol. 8, no. 9, 1055, 2020.
- [10] S. Shao, R. Yan, Y. Lu, P. Wang, and R. X. Gao, "DCNN-based multi-signal induction motor fault diagnosis," *IEEE Transactions on Instrumentation and Measurement*, vol. 69, no. 6, pp. 2658-2669, 2020.
- [11] D.-J. Choi, J.-H. Han, S.-U. Park, and S.-K. Hong, "Motor fault diagnosis in changed environments using K-means and CNN," *Journal of Institute of Control, Robotics and Systems*, vol. 26, no. 5, pp. 348-354, 2020.
- [12] N. Helberger, K. Karppinen, and L. D'Acunto, "Exposure diversity as a design principle for recommender systems," *Information, Communication & Society*, vol. 21, no. 2, pp. 191-207, 2016.
- [13] E. Piedad, Jr., Y.-T. Chen, H.-C. Chang, and C.-C. Kuo, "Frequency occurrence plot-based convolutional neural network for motor fault diagnosis," *Electronics*, vol. 9, no. 10, 1711, 2020.
- [14] C.-S. Wang, I. H. Kao, and J.-W. Perng, "Fault diagnosis and fault frequency determination of permanent magnet synchronous motor based on deep learning," *Sensors (Basel, Switzerland)*, vol. 21, no. 11, 3608, 2021.
- [15] K. Satpathi, Y. M. Yeap, A. Ukil, and N. Gedda, "Short-time fourier transform based transient analysis of VSC interfaced point-to-point dc System," *IEEE Transactions on Industrial Electronics*, vol. 65, no. 5, pp. 4080-4091, 2018.
- [16] Y. Cheng, G. Zhang, C. Yu, B. Peng, X. Wu, and F. Xu, "Application of short-time fourier transform in feeder fault detection of flexible multi-state Switch," *Journal of Physics: Conference Series*, vol. 1754, no. 1, 012106, 2021.
- [17] X. Dong, G. Li, Y. Jia, and K. Xu, "Multiscale feature extraction from the perspective of graph for hob fault diagnosis using spectral graph wavelet transform combined with improved random forest," *Measurement*, vol. 176, 109178, 2021.
- [18] D. Wang, Y. Zhao, C. Yi, K.-L. Tsui, and J. Lin, "Sparsity guided empirical wavelet transform for fault diagnosis of rolling element bearings," *Mechanical Systems and Signal Processing*, vol. 101, pp. 292-308, 2018.
- [19] Y. Sun, S. Li, and X. Wang, "Bearing fault diagnosis based on EMD and improved Chebyshev distance in SDP image," *Measurement*, vol. 176, 109100, 2021.
- [20] Y. F. Hu, and Q. Li, "An adjustable envelope based EMD method for rolling bearing fault diagnosis," *IOP Conference Series: Materials Science and Engineering*, vol. 1043, no. 3, 032017, 2021.
- [21] G. R. Naik, S. E. Selvan, and H. T. Nguyen, "Single-channel EMG classification with ensemble-empirical-mode-decomposition-based ICA for diagnosing neuromuscular disorders," *IEEE Transactions on Neural Systems and Rehabilitation Engineering*, vol. 24, no. 7, pp. 734-743, 2016.
- [22] Z. Qin, H. Chen, and J. Chang, "Signal-to-noise ratio enhancement based on empirical mode decomposition in phase-sensitive optical time domain reflectometry systems," *Sensors (Basel, Switzerland)*, vol. 17, no. 8, 1870, 2017.

- [23] X. Qiu, Y. Ren, P. N. Suganthan, and G. A. J. Amaratunga, "Empirical Mode Decomposition based ensemble deep learning for load demand time series forecasting," *Applied Soft Computing*, vol. 54, pp. 246-255, 2017.
- [24] Y. Ren, P. N. Suganthan, and N. Srikanth, "A novel empirical mode decomposition with support vector regression for wind speed forecasting," *IEEE Transactions on Neural Networks and Learning Systems*, vol. 27, no. 8, pp. 1793-1798, 2016.
- [25] Y. Meng, T. Liu, K. Liu, J. Jiang, R. Wang, T. Wang, and H. Hu, "A modified empirical mode decomposition algorithm in TDLAS for gas detection," *IEEE Photonics Journal*, vol. 6, no. 6, pp. 1-7, 2014.
- [26] V. K. Mishra, V. Bajaj, A. Kumar, and G. K. Singh, "Analysis of ALS and normal EMG signals based on empirical mode decomposition," *IET Science, Measurement & Technology*, vol. 10, no. 8, pp. 963-971, 2016.
- [27] J. Zhang, H. Tang, T. Wen, J. Ma, Q. Tan, D. Xia, X. Liu, and Y. Zhang, "A hybrid landslide displacement prediction method based on CEEMD and DTW-ACO-SVR-cases studied in the three gorges reservoir area," *Sensors (Basel, Switzerland)*, vol. 20, no. 15, 4287, 2020.
- [28] P. Meiyang, S. Jun, Y. Yuhao, L. Dasheng, X. Sudao, W. Shengli, and C. Jianjun, "Improved TQWT for marine moving target detection," *Journal of Systems Engineering and Electronics*, vol. 31, no. 3, pp. 470-481, 2020.
- [29] R. Agrawal, and P. Bajaj, "Comparative classification techniques for identification of brain states using TQWT decomposition," *Journal of Intelligent & Fuzzy Systems*, vol. 41, no. 5, pp. 5287-5297, 2021.
- [30] W. Zeng, Z. Lin, C. Yuan, Q. Wang, F. Liu, and Y. Wang, "Detection of heart valve disorders from PCG signals using TQWT, FA-MVEMD, Shannon energy envelope and deterministic learning," *Artificial Intelligence Review*, vol. 54, no. 8, pp. 6063-6100, 2021.
- [31] Y. Tian, J. Ma, C. Lu, and Z. Wang, "Rolling bearing fault diagnosis under variable conditions using LMD-SVD and extreme learning machine," *Mechanism and Machine Theory*, vol. 90, pp. 175-186, 2015.
- [32] H. Zhou, H. Li, T. Liu, and Q. Chen, "A weak fault feature extraction of rolling element bearing based on attenuated cosine dictionaries and sparse feature sign search," *ISA Transactions*, vol. 97, pp. 143-154, 2020.
- [33] H. Chen, J. Yan, N. U. R. Junejo, J. Qi, and H. Sun, "Sparse Representation Based on Tunable Q-Factor Wavelet Transform for Whale Click and Whistle Extraction," *Shock and Vibration*, vol. 2018, pp. 1-9, 2018.